## Opto-Electronics Review

# Design of external microtextures for efficient light outcoupling in OLEDs with different preferential orientation of emission dipoles

Milan Kovačič*

Faculty of Electrical Engineering, University of Ljubljana, Tržaška cesta 25, 1000 Ljubljana, Slovenia

| Article info | Abstract |
|---|---|
| | External light outcoupling structures provide a cost-effective and highly efficient solution for light extraction in organic light-emitting diodes. Among them, different microtextures, mainly optimized for devices with isotopically oriented emission dipoles, have been proposed as an efficient light extraction solution. In the paper, the outcoupling for a preferential orientation of emission dipoles is studied for the case of a red bottom-emitting organic light-emitting diode. Optical simulations are used to analyse the preferential orientation of dipoles in combination with three different textures, namely hexagonal array of sine-textures, three-sided pyramids, and random pyramids. It is shown that while there are minimal differences between the optimized textures, the highest external quantum efficiency of 51% is predicted by using the three-sided pyramid texture. Further improvements, by employing highly oriented dipole sources, are examined. In this case, the results show that the top outcoupling efficiencies can be achieved with the same texture shape and size, regardless of the preferred orientation of the emission dipoles. Using an optimized three-sided pyramid in combination with ideally parallel oriented dipoles, an efficiency of 62% is achievable. A detailed analysis of the optical situation inside the glass substrate, dominating external light outcoupling, is presented. Depicted results and their analysis offer a simplified further research and development of external light extraction for organic light-emitting devices with highly oriented dipole emission sources. |

## 1. Introduction

Organic light-emitting diodes (OLEDs) are widely used in display technology and are also spreading rapidly in wearable electronics, healthcare, and other fields [1, 2]. OLEDs also have a great potential to be used as a large-area solution for general lighting, as they offer uniform light distribution over large areas, are highly efficient, have high colour quality, and can be manufactured at low cost [2–5]. The ability to manufacture them on rigid or flexible substrates, as well as the ability to make them partially transparent open many possibilities for OLEDs in architecture and lighting design.

The potential of OLEDs lies in their high internal quantum efficiency (*IQE*), with the conversion of electrons to photons reaching close to 100%, which is a consequence of highly optimized OLED materials and structures [6, 7]. In contrast to high *IQEs*, the highest external quantum efficiencies (*EQEs*) for typical flat plane devices reach only 20 to 30% [8, 9]. This large gap is caused by inefficient light outcoupling and, consequently, optical parasitic losses in OLED structures. Primarily, this is a consequence of total internal reflections (TIRs) due to different refractive indices of the materials used. When light from a material with a high refractive index, $n$ (e.g., an organic emission layer $n \approx 1.7$–$1.8$) hits a material with a lower refractive index (e.g., a glass substrate with $n \sim 1.5$ or air with $n = 1$) at large angles (larger than the critical angle), it gets totally

*Corresponding author at: milan.kovacic@fe.uni-lj.si

internally reflected and, consequently, absorbed after many passes. Optical losses in OLEDs can be generally divided into three main groups. The first group consists of waveguide losses due to TIR at the internal organic layers or the transparent conductive oxide (TCO)/substrate interface. The second group are the so-called substrate losses due to TIR at the substrate/air interface (in case of bottom-emitting OLEDs). The third group consists of losses due to the coupling of light to the surface plasmon polaritons (SPPs) at the metal contact layers [8, 10]. TIR-related losses are then manifested in parasitic absorption losses in different layers of the structure. The first and third groups of losses can be assigned to internal losses, while the second group is called external or substrate optical losses.

Recent development in the field of light extraction has produced different highly efficient solutions, both in optimizing OLED internal and external optical losses – see for example the latest reviews on light outcoupling solutions in OLEDs [1, 11, 12]. In particular, much research has been done to limit substrate losses by attaching microlenses [13–16], scattering films [17–20], introducing scattering particles [21], or using microtextures [22–25]. These solutions provide high improvements at low cost and, generally, do not affect the electrical properties of the sensitive organic layers. Moreover, most internal solutions focus only on the extraction of light into the substrate, while external solutions can still play an important role for the final extraction of light from the substrate into air. One of these external solutions is based on microtextures introduced on top of the glass substrate, facing the air surrounding medium. The textures are usually realized by using textured foils such as microlens arrays, scattering films, different textures. In recent years, textures of different shapes and sizes have been proposed, exhibiting good extraction performance. The same approach has been successfully developed to optimize light in-coupling in organic solar cells [26] and perovskite solar cells [27]. The efficiency and analysis of these textures have mainly been researched for OLED devices with isotropic orientation of emission dipoles (emitter molecules), while the analysis and optimization of these external textures for highly oriented dipole sources, to the best of our knowledge, have not been performed extensively. This seems to be an important step forward, as much effort has been put into research and design of OLED devices with highly parallel alignments of the emitting dipoles [28–30]. The actual organic molecule orientation (dipole orientation) is in practical cases dependent on various factors and can be dependent, for example, on the emitter type, different deposition methods (solution or vacuum process), on controlling the substrate temperature during deposition, as well as on the actual molecule shape, size, and weight. For details on the origin of the molecule orientation based on small-molecule emitters see Ref. 31 and for emitters based on phosphorescent and TADF emitters see Ref. 30.

OLED devices with highly parallel orientation of emitting dipoles, if properly designed, exhibit high extraction of light from the thin-film stack and, if correctly optimized, also into the air. When these parallel emission dipoles are combined with external texturization, further improvements are possible, as it will be shown.

In this contribution, an analysis based on numerical simulations is carried out for a selection of three different forms of external microtextures: a hexagonal array of sinusoidal-(sine-)like texture, a hexagonal array of three-sided pyramids, and a random array of four-sided pyramids. The analysis of the above mentioned textures is made for OLEDs with differently oriented (from ideally vertical to ideally horizontal) dipole sources. Advanced optical simulations are used to evaluate and compare the effects of texture size and shape for optimized thicknesses of thin-film structures with a different preferential orientation of emission dipoles in the emission layer. A detailed analysis of the optical situation inside the OLED structure is modelled, enabling the optimisation and evaluation of both the thin-film structure and the attached microtextures for the optimal outcoupling of light considering the different preferential orientation of emitting dipoles. Optical properties inside the glass substrate, namely the light intensity distribution (LID), reveal the main properties that enable high outcoupling for differently oriented emitter molecules (point dipoles). In this regard, the usage of preferential alignments of the emitting dipoles in combination with external textures has been analysed and evaluated, showing a potential for very high optical efficiencies, especially for more parallel oriented emission dipoles. Therefore, an analysis of the performance of external texturization in combination with differently oriented emission dipoles, from ideally horizontal to ideally vertical orientations, is carried out.

## 2. Structures and methods

### 2.1. OLED structure

The main optical analysis in this contribution is done on an ITO-free, red bottom-emitting OLED. The structure offers a high *IQE* and, due to double metal contacts, enables the beneficial use of the formed optical cavity of the OLED device. The schematic representation of the OLED structure with functional layer names and corresponding thicknesses, as optimized for the optimal coupling of light to the glass substrate, can be seen in Fig. 1.
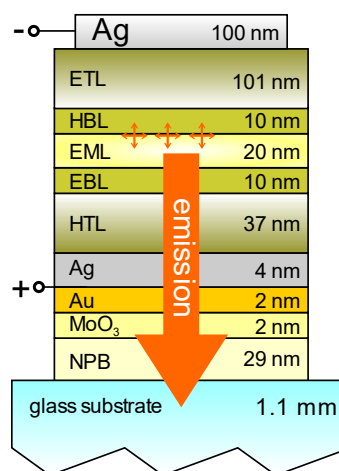


**Fig. 1.** Cross-sectional structure of a red bottom-emitting OLED with corresponding layer thicknesses as optimized for the optimal coupling of light into the glass substrate. External texturization was in the simulations considered as part of the glass substrate.

Light is generated by a radiative recombination of electrons and holes inside an organic emission layer (EML). Most of the radiative recombination occurs close to a hole-blocking layer (HBL) due to the preferential hole conductivity of EML, thus, the emission zone in simulations is considered as a lateral plane at the EML/HBL interface. EML is surrounded by HBL and electron-blocking layer (EBL) and hole- and electron-transmission layers (HTL and ETL) that enable a good supply of both electrons and holes and confine recombination inside the EML layer, enabling high internal efficiencies. Electric contacts are realized by a top opaque layer of Ag which is used as a cathode and reflector and an ultra-thin Ag (semi-transparent) layer which is used as an anode and semi-reflecting layer to form the cavity. Ultra-thin Ag anode is supplemented by additional Au and $MoO_3$ thin layers that are used to enable a uniform growth of the Ag layer [32, 33]. The entire thin-film structure is deposited onto a thick glass substrate with an additional buffer layer between the substrate and the thin-film stack (NPB) to improve adhesion of the stack to the glass substrate. On the other side of the glass substrate (opposite to the thin-film stack), different external textures can be applied, either by applying textured foils or by being directly fabricated, by, e.g., etching [34], laser processing of the glass [23], or by imprinting textures into transparent lacquers deposited on the glass substrate [27, 35, 36]. In the simulations, all textures are treated as part of the glass substrate, which is justified due to very similar optical properties of lacquer, textured foils, and a glass substrate. These exhibit negligible differences in refractive index, thus, as it was already shown in previous publications [22, 25], can be treated as a single layer.

To evaluate the outcoupling efficiency of different texturization, three different types of textures were included in the analysis. The analysed textures with selected lateral to horizontal feature dimension ratios are presented in Fig. 2 as: (a) – hexagonal array of sine-shaped textures, 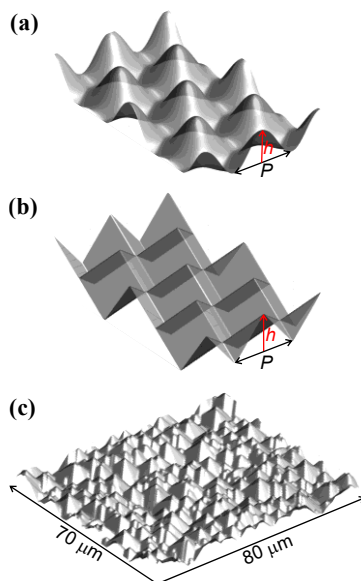(b) – a hexagonal array of special cube-shaped three-sided pyramid texture, and (c) – a random array of pyramids, such as obtained by transferring the texture of the etched c-Si surface.

Textures are described by its aspect ratio (AR), defined as a ratio between the height (h) and the period (P) of each texture, see Fig. 2. For the random pyramid texture, AR is defined by the pyramid angle (ϑ), where $AR = \tan(\vartheta)$. For presented textures, AR is varied between 0 and ~2, according to the actual texture by changing the texture h, while the lateral dimensions (P) are held constant. As dimensions of selected textures are already in the geometric optics regime, thus, only AR and not actual P and h are influencing the outcoupling. All presented textures can be fabricated separately on foils and attached to the glass substrate or can be fabricated directly on foils or lacquer layers after their attachment or deposition on glass substrates by, e.g., an ultraviolet nanoimprint lithography (UV-NIL).

### 2.2. Models

The EQE is a commonly used parameter to evaluate opto-electrical efficiency of OLED devices and is defined as a ratio between the number of photons reaching the far field (usually measured in the air) to the number of injected charge carriers in the device. EQE can be also calculated using (1), where $IQE = \gamma * \eta^*_{rad,e}(\lambda)$ is the internal quantum efficiency combining $\gamma$ – the electrical efficiency defined as a ratio between the number of radiative recombinations in the emission layer and the number of injected charge carriers, and $\eta^*_{rad,e}(\lambda)$ is the effective radiative efficiency

$$EQE = IQE \int_{\lambda} s_{el}(\lambda)\, \eta_{out}(\lambda) d\lambda\,, \qquad (1)$$

where $s_{el}(\lambda)$ is the normalized electroluminescent spectrum of emission material and $\eta_{out}(\lambda)$ is the outcoupling efficiency. In this contribution, the focus is only on the optimization of light outcoupling, thus IQE of the OLEDs is treated as ideal, $\gamma = 1$ and $\eta^*_{rad,e}(\lambda) = 1$. This is justified, as there are numerous reports on OLED devices with internal (electron to photon conversion) efficiencies close to 100% [37–39]. This simplifies (1) to

$$EQE = \int_{\lambda} s_{el}(\lambda)\, \eta_{out}(\lambda) d\lambda\,. \qquad (2)$$

Here, now only the light outcoupling and the emission spectrum define the efficiency. Using (2), only the optical properties (considering idealized electrical properties) of the device are indicated. Although in this contribution only the improvement of optical properties is considered, it needs to be noted that any change to the OLED structure was done in such a way that it would not deteriorate electrical properties, keeping internal efficiencies high.

In EML, the electroluminescence emission occurs inside emitter material molecules. The sizes of these molecules are considerably smaller (in the range of several nanometres) than the emitted light wavelength (visible light), thus in optical simulations, these can be treated as



**Fig. 2.** Selected external textures as used in simulations: a hexagonal array of sine shaped textures – P = 10 mm (a), a hexagonal array of a special cube-like three-sided pyramid texture – P = 7.82 mm (b), and a random array of pyramids as scanned from the surface of crystal Si (c).

point dipole sources. The orientation of molecules (dipoles) can be represented by a combination of three perpendicular dipoles, two horizontally and one vertically oriented, according to the selected global coordinate system. In most cases, the orientation of dipoles in the plane of a layered system is treated as isotopically oriented [40], thus only the ratio between vertical and horizontal dipoles is considered. This ratio is quantified by the anisotropy coefficient $a$ which is defined as the ratio between the vertical dipole component towards all three dipole components and is used to describe the general orientation of all emitting dipoles in the device. For example, anisotropy factor $a = 0.33$ would mean isotropic orientation of emitting dipoles with all three components being equally represented, for $a = 0$ all dipoles would be horizontally orientated, and for $a = 1$ all dipoles would be vertically orientated. For the presented OLED device, an initial $a$ of 0.24 is considered, having a slightly preferential horizontal orientation of emitting dipoles.

OLED devices consist of optically thin (thicknesses in the range of a wavelength) organic layers with contacts and optically thick (thicknesses in the range of several μm to mm) substrate, and encapsulation layers. In optically thin layers, light is treated as waves and in optically thick ones, light is treated as rays, thus different modelling approaches for simulations need to be considered. In the utilized model, a modified transfer matrix method (TMM) is used to model light emitting sources [23]. Emission sources are simulated as a classical, continuously oscillating dipoles with a predefined spectrum and angular intensity distribution. In the TMM formalism, the angular light intensity distribution is converted through Fourier decomposition into plane waves travelling under specified angles. According to the dipole orientation to the interfaces of the planar system, corresponding planar waves reach the interfaces at different incident angles, where, according to its electric and magnetic field components, TE and TM polarizations are identified. A predefined light intensity distribution, according to the dipole orientation, with corresponding TE and TM components is used in the simulations. Azimuthal orientation of dipoles, due to the random orientation of the emitting dipoles in the plane of layers [40], is treated as isotropically oriented.

Dipole sources are positioned inside the emission layer of the OLED organic stack, which is considered in the simulations as a locally flat thin-film stack with parallel coherent layers. Such stack is optically described by layer thicknesses and corresponding wavelength-dependent refractive indices. TMM is used to describe light emission, as well as coherent light waves propagation inside the thin-film structure of OLED. TMM enables inclusion of both interference and microcavity effects, as well as evanescent waves and coupling of light to surface plasmon polaritons, allowing an accurate simulation of the optical situation.

TMM can be used only for plane parallel structures, which is the case for most typical OLED structures, including the analysed one in this contribution where no additional scattering effects are considered. More complex structures incorporating lateral disruptions (e.g., scattering particles, texturization) require a more advanced simulation method to be used (e.g., FEM [41], FDTD [42]). For modelling of the light propagation and refraction in an optically thick substrate (and other thick layers), a 3D raytracing approach is used [43] which enables the inclusion of a sufficiently large (compared to the light wavelength) micro-sized texturization.

Waves exiting the thin-film stack are converted into incoherent rays considering the real part of the Poynting vector with their intensities and directions. Thus, in the thick layers of the OLED structure (such as glass substrate and light management foil), the light is represented by incoherent rays. The polar angles are determined through the actual orientation of the emitting dipoles as determined using TMM. Rays are then traced through the thick layer(s) where they are reflected, transmitted, or refracted at flat or textured interfaces until they are extracted to the far field (air) or absorbed in the structure. For rays entering the same or different thin-film stack, TMM is again used to calculate the reflection, transmission, and absorption of the stack, with possible reflected and transmitted parts of light being again transformed back to the rays. Full details of the used combined model can be found in Ref. 23 with the experimental verification of the full model in Refs. 22, 23, and 25.

Optimization of the thin-film layer thicknesses was performed using the "patternsearch" optimization function, integrated in the MATLAB environment [44]. This function searches for local minima only, so an additional "MultiStart" function was used to assure that a global minimum was found in the specified range. A discrete thickness step of 1 nm was used in the optimization. Optimization of the external texture, on the other hand, was performed by individual simulations of each texture with multiple *AR* values in the selected range. In this way, a full set of values was obtained from which optimal *AR*s and corresponding *EQE*s are easily extracted.

## 3. Results

Using the presented model, simulations were performed to obtain the highest outcoupling of light for different OLED configurations, in particular: 1) optimization of a thin-film layer stack with flat interfaces only, to gain the highest coupling of light into the glass substrate (also air); 2) optimization of the texture shape and size, with a constant thin-film stack; 3) optimizations of 1) and 2) but using different preferential orientations of the emitting dipoles. Optimization of thin-film layers was confined to buffer layer (NPB), front contact layers (MoO$_3$, Au, Ag), and both transport layers (HTL, ETL). Changing thicknesses of both transport and buffer layers has only minimal effect on the electrical properties of the OLEDs and can thus be arbitrarily changed. Front contact and supporting layers need to have minimal thicknesses, with both supporting layers (Au and MoO$_3$) being at least of 2 nm, which is sufficient for a uniform growth of Ag. The Ag front contact layer requires to be at least 4-nm thick to ensure good contact properties. A minimum step in layer thickness was limited to 1 nm which is already below or in the range of common manufacturing tolerances (e.g., spin coating, sputtering). Additionally, simulation results show that changes less than 1 nm exhibit almost negligible differences in optical properties.

Texture optimization was done by changing the *AR* of each texture. For each texture, the period of the texture was kept fixed and only the height of the texture varied. By this, *AR* varied from 0 – flat to higher values, depending on the

individual texture. For random pyramids, *AR* was determined according to the pyramid angle.

### 3.1. Optimization of the device thin-film structure

First, layer thicknesses for OLED devices without any texturization and with different preferential dipole orientations were optimized for the highest light extraction. Simulation results show that an optimal *EQE* of 35% can already be achieved without external outcoupling solutions. If a different preferential orientation of the dipoles is proposed, the *EQE* (outcoupling) can increase up to 48% for ideally parallel dipoles and down to 12.8% for ideally vertically oriented dipoles. Table S1 in supplementary information (SI) lists the optimal thicknesses of the optimized layers for selected orientations (from ideal horizontal $a = 0$, isotropic $a = 0.33$, to ideal vertical $a = 1$) and the corresponding *EQE*s. These results are used as a reference for all further optimizations. This evaluation is appropriate since texturization can improve the *EQE* of poorly designed OLEDs (optical cavity) many times over, while the final *EQE* can still be much lower than for an optimized device without texturization. In this respect, any improvement in outcoupling due to texturization must be related to the optimized flat plane devices.

Next, the thicknesses of the thin-film OLED stack are first optimized to ensure the optimal coupling of the light into the glass substrate. This optimization is necessary because external structures can only extract the light that reaches the substrate. In the next step, optimization of the external texture is performed in order to extract as much light as possible from the substrate to the surrounding air.

These optimized thin-film structures, which take into account different preferential orientations of the emitting dipoles, also allow a direct comparison between different textures in the case of a fixed thin-film structure, since only the texture changes while all other layers and properties remain constant. Here, for a standard $a = 0.24$, up to 65% of the light can be extracted from the thin-film structure into the glass substrate, while for ideally horizontal dipoles up to 80% of the light can be extracted from the thin-film structure. In this case, the optimal layer thicknesses – see Table 1 (and extended Table S2 in SI) – are significantly different from those in the optimized flat plane device with glass/air interface (SI – Table S1), indicating the importance of optimizing the thin-film layer stack according to the outcoupling strategy. In this case, the front contact layers (MoO$_3$, Au, Ag) are at their minimum values and remain unchanged regardless of the value of *a*. In contrast to the structure with a glass/air interface, the strong cavity effect becomes less important here, since high transmission at a lower angle is no longer essential (no critical angle at the glass/air interface), but only high transmission into the glass substrate at any angle is beneficial. This results in minimizing the thickness of the highly absorbing front contact layers, reducing parasitic absorption, and allowing a high amount of light to reach the substrate. Moreover, only small thickness changes are observed for the HTL layer, while much larger differences in the optimal thicknesses are visible for the ETL layer, changing from 78 nm for an ideally parallel ($a = 0$) to 111 nm for an isotropic ($a = 0.33$) orientation. Evidently different values can be observed in the optimal layer thicknesses for strongly vertically oriented ($a = 1$) dipoles – see Table 1. Vertically oriented dipoles emit only TM oriented light and, therefore, exhibit higher SPP losses which decrease with distance from the metal contacts. This results in thicker transport layers that shift the emission further away from the metal contacts, minimizing SPP losses and consequently allowing more light to be outcoupled.

Table 1
Optimal *EQE* and corresponding optimized layer thicknesses for the optimal coupling of light into the glass substrate, considering an ideal extraction from the glass substrate into air. In simulations, the glass substrate is considered as half-infinitive.

| Anisotropy | $a = 0.24$ | $a = 0$ | $a = 0.33$ | $a = 1$ |
|---|---|---|---|---|
| *EQE* | 0.65 | 0.80 | 0.60 | 0.50 |
| **Layer (nm):** | | | | |
| NPB | 29 | 47 | 18 | 152 |
| MoO$_3$ | 2 | 2 | 2 | 2 |
| Au | 2 | 2 | 2 | 2 |
| Ag | 4 | 4 | 4 | 5 |
| HTL | 37 | 39 | 37 | 170 |
| ETL | 101 | 78 | 111 | 213 |

### 3.2. Optimization of texturization for OLED stacks with different orientations of dipole sources

All presented textures were used with the same OLED structure optimized for the optimal coupling of light to the glass substrate and their effect on *EQE* was evaluated. Outcoupling efficiency was simulated for three selected distinctive orientations of dipoles with $a = 0$, 0.33, and 1, presenting ideally parallel, isotropic, and ideally vertical orientation of emission dipoles, respectively. For each selected anisotropy value, *EQE* was simulated with respect to the *AR* texture at constant period. The resulting *EQEs* depending on *AR* for the selected textures can be seen in Fig. 3.



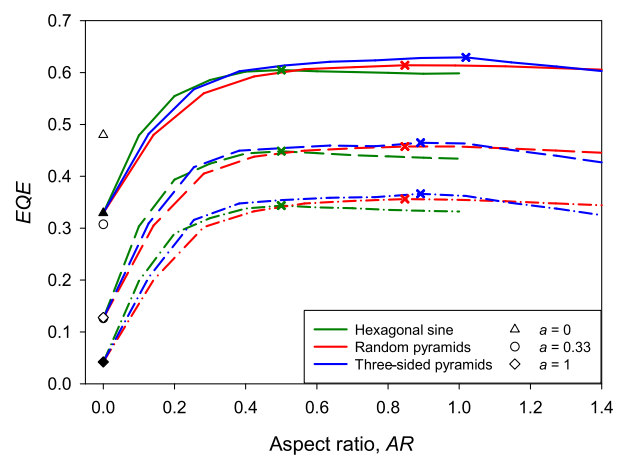**Fig. 3.** *EQE* (outcoupling efficiency) by using selected textures – see Fig. 2, depending on the *AR* texture for three different preferential dipole orientations ($a = 0$, 0.33, and 1). Added solid black symbols indicate outcoupling without texturization (thin film optimized for coupling into the glass substrate) and empty black symbols indicate *EQE* for the optimized flat device.

The results in Fig. 3 show that, regardless of the texture and *a* value, *EQE* increases with increasing *AR* of the textures up to a certain level where it reaches a saturation, followed by a small decrease at large *AR*. For all textures, the saturation plateau with the highest *EQE* is quite broad and tolerates some variation in production, allowing for lower quality and, thus, possibly faster, cheaper, and high throughput production of external textures.

In Fig. 4, a comparison of the levels of the highest *EQE*s is presented. Results are obtained at optimal *AR*s for different textures and for different *a* values, as can be extracted from Fig. 3. The highest *EQE*s (for initial *a* = 0.24) of 44.8%, 45.8%, and 46.5% are predicted for sine-texture (*AR* = 0.5), random pyramid (*AR* = 0.85) and three-sided pyramid (*AR* = 0.9), respectively.
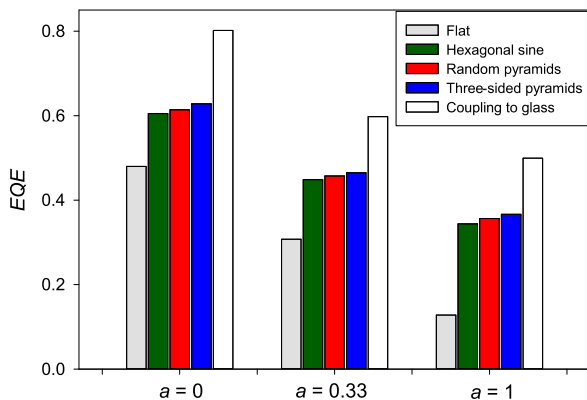


**Fig. 4.** Comparison of *EQE* for the selected optimized textures for three different dipole orientations. White columns represent total amount of light coupled to the glass substrate for each anisotropy value, colour columns represent actual amount of light extracted to air, and gray columns indicate the highest outcoupling for the optimized flat device.

All analysed textures achieve a comparably high *EQE*s with only small differences of ~2% between them. High *EQE*s are mainly independent of the actual texture shape, while only high enough *AR* of textures needs to be achieved. These results are consistent with the findings in Ref. 14, where for a good outcoupling, textures that sufficiently redirect rays are needed, while the texture shape itself is not that important. On the other hand, there are differences, albeit small, between individual textures. The lowest *EQE* for a standard OLED (*a* = 0.24) is predicted when the optimized sine-textures in a hexagonal arrangement are used, and the highest is predicted when the three-sided pyramidal textures are used. The absolute difference is in the range of ~2% from 48.9% to 50.9%. Similar trends can also be observed for other preferential orientations of the dipoles. Again, the best results are observed for the three-sided pyramids and the lowest for the hexagonal sine-texture, regardless of the preferential orientation of the dipoles – see Fig. 4. Moreover, the highest *EQE*s are obtained at approximately the same *AR* of each texture, regardless of the preferential orientation of the dipoles – see Fig. 3. This suggests that the *EQE*s of the external textures are almost independent of the preferential orientation of the emitting dipoles. This can be very advantageous as no further optimization of the texture is required for devices with different preferential dipole orientations since the same texture provides the optimal outcoupling regardless of the dipole orientations. On the other hand, optimization of the thin-film layers still plays an important role and has to be treated separately for each orientation. Results also indicate that many efficient external outcoupling solutions already developed for devices with isotropic orientation could also allow for close to optimal outcoupling for devices with a different preferential orientation of the dipoles without the need to change them.

Comparison of the absolute *EQE*s in Fig. 4 for different preferential orientations of the dipoles shows that the highest values are obtained for strongly parallel oriented dipoles and the lowest values for strongly vertically oriented dipoles. The main reason for these differences is in the amount of light reaching the substrate itself and is thus available for extraction. This amount is the highest for horizontally aligned dipoles (~80%) and the lowest for vertically oriented dipoles (~50%) – see white bars in Fig. 4. Beside this, an additional analysis is performed where the relative extraction from the glass substrate was calculated for each orientation tested. These results show that the highest amount of light extracted from the substrate is with horizontally aligned dipoles (for three-sided texture ~78%), while the lowest amount is extracted with vertically aligned dipoles (for three-sided texture ~69%). Since the horizontal orientation of dipoles enables more light to reach the substrate and is thus available for extraction, this combined with a higher extraction efficiency for horizontally oriented dipoles results in a higher overall extraction efficiency, making preferentially horizontally oriented dipole sources highly desirable from an optical point of view for use in OLED devices.

## 4. Discussion

Additional simulations and analysis of internal optical situation in the structure have been performed to explain and discuss the presented results in the previous section.

### 4.1. Light outcoupling process

As investigated in Ref. 25, the light outcoupling depends essentially on the angle-dependent transmission (*T*) from the glass substrate to the air. For the flat glass/air interface, a pronounced dependence is observed with a high transmittance at small angles – below the critical angle – and a transmittance of 0 at angles greater than the critical angle – see black line in Fig. 5.

This means that for flat interfaces, where there is no redirection of rays at the texture, all light travelling at angles larger than the critical angle is waveguided until it is absorbed in the structure. A comparison of *T* towards different light intensity distributions (LIDs) in the glass substrate (optimized for the maximum coupling to the glass substrate for different *a* values) – see grey lines in Fig. 5 – shows that a large fraction of the light in the glass substrate travels at angles greater than the critical angle. This is particularly evident for highly vertically oriented sources (larger anisotropy values), resulting in a larger portion of the light being totally internally reflected and thus lost. When a thin-film structure is optimized for flat interfaces, the LIDs in the glass substrate changes so that more light travels under critical angle where it can be extracted. In the
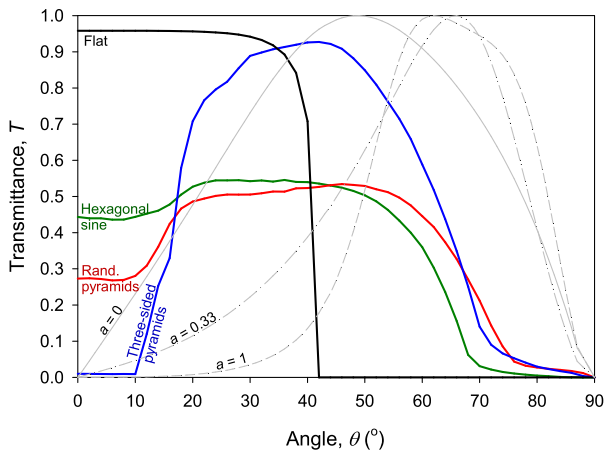
**Fig. 5.** Simulated angular-dependent transmittance of the glass/air structure for different texturizations at the interface (and flat interface). Added grey lines present normalized angular intensity distributions of monochromatic ($\lambda = 610$ nm) light for three anisotropy values, as present in the glass substrate before the first pass through the glass/air interface.

present case, this can be achieved by a thicker front Ag layer, which increases the cavity effect and leads to a more favourable LID in the glass (see SI – Fig. S1). On the other hand, this comes at the cost of less light reaching the substrate itself. Therefore, a balanced optimization is essential – see optical losses in layers for different optimized cavities in SI – Table S3.

When introducing external textures, it can be observed that the textures change the angular dependency of $T$ at the glass/air interface – see the colour lines for the optimized textures in Fig. 5. Lower transmittance can be observed at smaller angles, which is especially evident for three-sided pyramids, where $T$ drops almost to 0 at angles below 10 degrees. On the other hand, a much higher $T$ value can be observed at larger angles, above the critical value, allowing the extraction of light at larger angles. The comparison of $T$ as a function of the incident angle for the selected textures shows considerable differences in the angle-dependent $T$, while the final outcoupling efficiency, for the selected dipoles orientation, differs only slightly. This suggests that the non-zero $T$ value for larger angles, common to all textures, now leads to the ability of light outcoupling at larger angles which in combination with the redirection of back reflected rays (from the texture) results in a high outcoupling efficiency when these rays come again to the interface, after being reflected in the OLED stack. On the other hand, a decreased or increased transmittance does not seem to have much effect on smaller angles, which is consistent with the results in Ref. 25. A much higher $T$ for three-sided pyramids at angles around the critical angle gives an advantage over other textures in light extraction. This is particularly evident in the first and second pass of the texture, where the three-sided pyramid texture transfers more power to the air compared to other textures tested – see SI – Fig. S2 for the stepwise power transfer from the glass substrate to the air.

### 4.2. Effect of dipole orientation on outcoupling

The use of essentially the same optimal texture shape and size results in the optimal outcoupling efficiency regardless of the preferential dipole orientation. However, the level of outcoupling is different for different dipole orientations. To investigate and explain the effects related to different dipole orientations in combination with external textures, the internal LIDs related to different structures were checked. Remarkable differences in the initial internal LID in the glass substrate (as extracted from the thin-film structure) can be observed for differently oriented emission dipoles – see grey lines in Fig. 5. To investigate this further, a detailed analysis of the optical situation inside the structure was carried out by preforming a step-by-step analysis of light transmission from the glass substrate into the air. Here, special simulations were performed where light emitted from a thin-film structure with specific LIDs was sent through the glass/air interface. All the reflected light was then collected and its intensity was reduced for corresponding reflection loss due to the actual angle and polarization-dependent thin-film structure reflection losses. This light with the new LID and polarization was sent through the glass/air interface again, repeating the process for the first 8 texture passes. In this way, outcoupling can be evaluated as a function of texture pass, indicating the outcoupling of individual texture/air transmission and not only a total transmission. Results of this analysis are shown in Fig. 6.
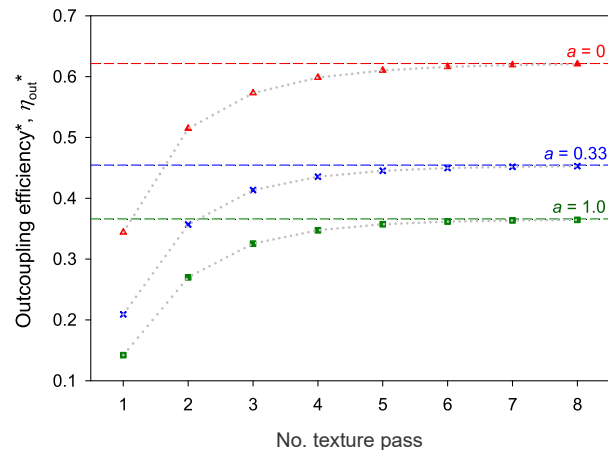


**Fig. 6.** Simulated outcoupled power of light in the air shown sequentially as a function of the texture pass number. For light with $\lambda = 610$ nm for the optimal ($AR = 0.9$) three-sided pyramid texture. Dashed grey lines serve as a guide to the eye. More than 99% of the light gets extracted in the first 8 texture passes. Outcoupling efficiency* is here considered as the cumulative outcoupling sum after each texture pass.

Results indicate that most of the light is outcoupled already in the first 6–8 texture passes, where more than 99% of the light is either outcoupled or lost (absorbed) – see Fig. 6. It can also be observed that external textures do not outcouple light only at the first pass, but a large fraction of the light is reflected (50–70%) and outcoupled at the subsequent passes of the texture. As light gets reflected from the textured glass/air interface due to the ray redirection, its LID also changes which, in turn, influences $T$ properties and, consequently, the outcoupling at subsequent passes of the textured glass/air interface. In this context, LID is analysed in the glass substrate at different event points. Simulations for three different initial LIDs in the substrate (corresponding to the different anisotropy orientations) reflected from the optimized three-sided pyramid texture can be seen in Fig. 7.
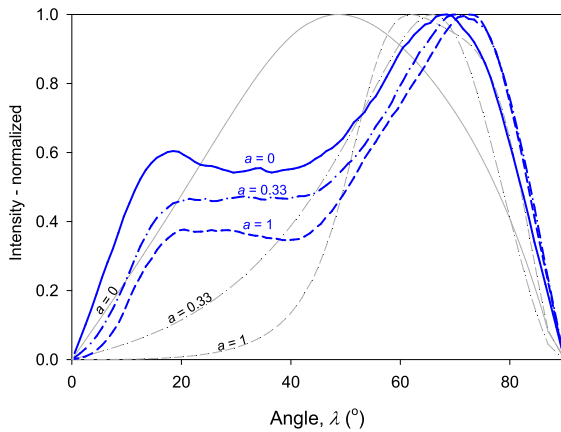
**Fig. 7.** Simulated LID after being reflected from the textured glass/air interface for the optimized three-sided pyramid texture ($AR = 0.9$) and different anisotropy values for the first time. LIDs of monochromatic ($\lambda = 610$ nm) light are added for three anisotropy values, as present in the glass substrate before the first pass through the glass/air interface, showing that highly different initial LIDs transform into very similar reflected LIDs.

Results show that reflected light produces very comparable LIDs already after the first reflection. As seen in Fig. 7, LIDs, after the first reflection from the textured interface, show highly comparable LIDs regardless of the initial LIDs of the differently oriented dipoles. Since the texture extracts light not only in the first pass, but also in large amounts in all subsequent passes, a sufficient redirection of the rays already in the first pass of the texture sufficiently redirects rays and changes LID, so that the subsequent LIDs for all subsequent passes are quite similar and the large differences of the first LIDs are eliminated. This results in a comparable outcoupling regardless of the anisotropy values and the corresponding different initial optical properties.

### 4.3. Effects of dipole orientation on extracted spectrum and LID

Modifications of the optical microcavity due to different dipole orientations can change not only the light intensity distribution but also the actual extracted spectrum. This is especially evident for an ideally flat device due to the strong cavity effect (thick front metal contact), where a spectrum peak shift, as well as a widening or narrowing of the extracted spectrum can be observed depending on the preferential orientation of the emission dipoles [see SI – Fig. S3(a)]. Moreover, spectrum can be additionally changed according to the observation angle in this case, which can have highly negative effect, especially for white devices, where colour can change depending on the observation angle. For devices optimized for optimal coupling of light into the glass substrate, this effect is much less pronounced as the cavity effect is reduced (thinner front metal layer). When combined with the texturization, due to the strong ray redirection, changes in the extracted spectrum between different dipole orientations are further diminished, exhibiting a highly similar spectral response [SI – Fig. S3(b)].

Depending on the orientation of the emission dipoles, the light generated can have different ratios of TE and TM polarized light. Devices with flat interfaces do not exhibit

changes in light polarization from emission to exit medium, e.g., for ideally vertically oriented dipoles only TM polarized light is emitted and only TM reaches the far-field medium. In the case of textured devices, light falling on the textured interface gets redirected and can change the ratio of TE and TM light. For example, in the case of an ideally vertical orientation of dipoles, where the dipoles emit only TM polarized light, the final polarization of the extracted light (in air) is not only TM, but a combination of both TM and TE with only a small amount of TM prevailing [see SI – Fig. S4(c)]. For isotropically and ideally horizontal orientation of the emitting dipoles, where the already generated light is a combination of TE and TM polarized light, the final extracted ratio of TE *vs*. TM is in equal proportions [see SI – Figs. S4(a) and (b)].

### 4.4. Different OLED structures

So far, only the results for OLED devices with double metal contacts have been presented, but the results and findings presented here also apply to other structures, such as OLEDs based on transparent conductive oxides (e.g., indium tin oxide – ITO). To confirm this, the same optical analysis as presented above was done also for the similar OLED structure where only the metal anode stack has been replaced by a 90-nm thick ITO (NPB/MoO$_3$/Au/Ag => ITO). The results for this red bottom-emitting OLED with an ITO anode show very similar outcoupling trends, both in terms of optimal texture and anisotropy dependence. Here, the same texture (three-sided pyramids) with the same optimal $AR$ as in the case of the OLED with a double metal contact is optimal for the highest outcoupling. Results also show that, for this device, there is minimal to no difference in the shape and size of the texture where the highest outcoupling is achieved when different preferential orientations of the dipoles are used. SI – Fig. S5 shows the simulation results of the $EQE$ dependence on $AR$ for a three-sided pyramid and for different $a$ values for an ITO-based OLED. On the other hand, the highest outcoupling efficiencies are lower than the ones of OLED with a double metal contact due to the different composition of devices. Using the optimized three-sided pyramids, the highest outcoupling efficiency ($a = 0.24$) of $EQE = 39.9\%$ is predicted for OLEDs based on ITO, compared to an $EQE$ of 50.9% for OLEDs with double metal contacts, indicating the superiority of OLEDs with double metal contacts.

### 5. Conclusions

Enhanced outcoupling of light in a bottom-emitting OLED device with different external textures was researched for structures with different source dipole orientations. Three types of external textures, namely hexagonal array of sine-textures, three-sided pyramid textures, and random pyramid textures were used as external outcoupling solutions for the case of a large-area, red bottom-emitting OLED devices. Optical modelling was used to evaluate and analyse the outcoupling properties of the presented textures, additionally considering the different preferential orientation of the emitting dipoles and the corresponding OLED thin-film design – optical cavity optimization.

The potential of different texturization for light extraction by changing their aspect ratios was investigated. All the textures used show a strong dependence on the aspect ratio of the texture and achieve the optimal outcoupling efficiency when a sufficiently high *AR* is used. The highest *EQE* of 50.9% is predicted when using the optimized three-sided pyramidal textures. Moreover, all optimized (with sufficiently high *AR*) textures show the high outcoupling efficiency (~49–50% *EQE*), indicating very little dependence on the outcoupling ability according to the actual texture shape (sine, pyramid).

The presented external textures were also tested for use with strongly oriented dipole sources, with the highest overall *EQE*s predicted for highly horizontally ($a = 0$) oriented dipoles. The results show that the thickness optimization for the given dipole orientation of the thin-film stack is very important to achieve the highest efficiency, while on the other hand, the dependence on the texture type is very low. It was shown that the same textures with the same properties (aspect ratio) exhibit the highest outcoupling efficiency regardless of the preferential dipole orientations. This is extremely beneficial as it eliminates the need for additional texture optimization for devices with different preferential dipole orientations. Optimized textures for any preferential orientation of the emitting dipoles allow for the highest outcoupling regardless of the preferred dipole orientations, given the optimized thin-film stack. In addition, many already developed and efficient external outcoupling solutions for devices with isotropic orientations should also provide the optimal outcoupling for devices with alternative preferential orientation of the dipoles.

A detailed analysis of the outcoupling properties by using different textures was performed and the most important properties for efficient light outcoupling were identified. In addition to the high coupling of light into the glass substrate, from where light can be extracted using the presented textures, a high light transmission from the glass substrate into the air at larger angles, around critical and larger angles, is essential. Moreover, high *EQE*s are predicted for highly parallel aligned emission dipoles, which inherently allow larger amounts of light to reach the glass substrate and, also, which results in higher extraction efficiencies compared to more vertically aligned dipoles.

Overall, the highest extraction efficiencies are predicted when the same optimized three-sided pyramidal texture is used in combination with any type of preferential orientation of the emitting dipoles. Further research and development of ideally parallel aligned dipoles is highly desirable, as they would allow for a high *EQE* of more than 62% when combined with the three-sided pyramid texture.

## Acknowledgements

## References

[1] Song, J., Lee, H., Jeong, E. G., Choi, K. C. & Yoo, S. Organic light-emitting diodes: pushing toward the limits and beyond. *Adv. Mater.* **32**, 1907539 (2020). https://doi.org/10.1002/adma.201907539

[2] Yin, Y., Ali, M. U., Xie, W., Yang, H. & Meng, H. Evolution of white organic light-emitting devices: from academic research to lighting and display applications. *Mater. Chem. Front.* **3**, 970–1031 (2019). https://doi.org/10.1039/C9QM00042A

[3] Pode, R. Organic light emitting diode devices: An energy efficient solid state lighting for applications. *Renew. Sust. Energy Rev.* **133**, 110043 (2020). https://doi.org/10.1016/j.rser.2020.110043

[4] Chang, Y. & Lu, Z. White organic light-emitting diodes for solid-state lighting. *J. Disp. Technol.* **9**, 459–468 (2013). https://doi.org/10.1109/JDT.2013.2248698

[5] Reineke, S., Thomschke, M., Lüssem, B. & Leo, K. White organic light-emitting diodes: Status and perspective. *Rev. Mod. Phys.* **85**, 1245–1293 (2013). https://doi.org/10.1103/RevModPhys.85.1245

[6] Hong, G. *et al.* A brief history of OLEDS—emitter development and industry milestones. *Adv. Mater.* **33**, 2005630 (2021). https://doi.org/10.1002/adma.202005630

[7] Adachi, C., Xie, G., Reineke, S. & Zysman-Colman, E. Editorial: recent advances in thermally activated delayed fluorescence materials. *Front. Chem.* **8**, 625910 (2020). https://doi.org/10.3389/fchem.2020.625910

[8] Forrest, S. R., Bradley, D. D. C. & Thompson, M. E. Measuring the efficiency of organic light-emitting devices. *Adv. Mater.* **15**, 1043–1048 (2003). https://doi.org/10.1002/adma.200302151

[9] Furno, M., Meerheim, R., Hofmann, S., Lüssem, B. & Leo, K. Efficiency and rate of spontaneous emission in organic electroluminescent devices. *Phys. Rev. B* **85**, 115205 (2012). https://doi.org/10.1103/PhysRevB.85.115205

[10] Meerheim, R., Furno, M., Hofmann, S., Lüssem, B. & Leo, K. Quantification of energy loss mechanisms in organic light-emitting diodes. *Appl. Phys. Lett.* **97**, 253305 (2010). https://doi.org/10.1063/1.3527936

[11] Salehi, A., Fu, X., Shin, D.-H. & So, F. Recent advances in OLED optical design. *Adv. Funct. Mater.* **29**, 1808803 (2019). https://doi.org/10.1002/adfm.201808803

[12] Gather, M.C. & Reineke, S. Recent advances in light outcoupling from white organic light-emitting diodes. *J. Photonics Energy* **5**, 057607 (2015). https://doi.org/10.1117/1.JPE.5.057607

[13] Möller, S. & Forrest, S. R. Improved light out-coupling in organic light emitting diodes employing ordered microlens arrays. *J. Appl. Phys.* **91**, 3324–3327 (2002). https://doi.org/10.1063/1.1435422

[14] Greiner, H. Light extraction from Organic Light Emitting Diode substrates: simulation and experiment. *Jpn. J. Appl. Phys.* **46**, 4125 (2007). https://doi.org/10.1143/JJAP.46.4125

[15] Bae, H., Kim, J. S. & Hong, C. Simulation for light extraction efficiency of OLEDs with spheroidal microlenses in hexagonal array. *Opt. Commun.* **415**, 168–176 (2018). https://doi.org/10.1016/j.optcom.2018.01.044

[16] Zhou, J.-G., Hua, X.-C., Huang, C.-C., Sun, Q. & Fung, M.-K. Ideal microlens array based on polystyrene microspheres for light extraction in organic light-emitting diodes. *Org. Electron.* **69**, 348–353 (2019). https://doi.org/10.1016/j.orgel.2019.03.051

[17] Zhai, G., Zhu, W., Huang, L., Yi, C. & Ding, K. Enhanced light extraction from green organic light-emitting diodes by attaching a high-haze random-bowls textured optical film. *J. Phys. D: Appl. Phys.* **53**, 435101 (2020). https://doi.org/10.1088/1361-6463/ab9fc3

[18] Yen, J.-H., Wang, Y.-J., Hsieh, C.-A., Chen, Y.-C. & Chen, L.-Y. Enhanced light extraction from organic light-emitting devices through non-covalent or covalent polyimide–silica light scattering hybrid films. *J. Mater. Chem. C* **8**, 4102–4111 (2020). https://doi.org/10.1039/C9TC06449D

[19] Gasonoo, A. *et al.* Outcoupling efficiency enhancement of a bottom-emitting OLED with a visible perylene film. *Opt. Express* **28**, 26724–26732 (2020). https://doi.org/10.1364/OE.397789

[20] Song, J. *et al.* Lensfree OLEDs with over 50% external quantum efficiency via external scattering and horizontally oriented emitters. *Nat. Commun.* **9**, 3207 (2018). https://doi.org/10.1038/s41467-018-05671-x

[21] Tu, T. T. K. *et al*. Enhancement of light extraction from Organic Light-Emitting Diodes by SiO2 nanoparticle-embedded phase separated PAA/PI polymer blends. *Mol. Cryst. Liq. Cryst.* **686**, 55–62 (2019). https://doi.org/10.1080/15421406.2019.1648036

[22] Kovačič, M. *et al*. Coupled optical modeling for optimization of Organic Light-Emitting Diodes with external outcoupling structures. *ACS Photonics* **5**, 422–430 (2018). https://doi.org/10.1021/acsphotonics.7b00874

[23] Kovačič, M. *et al*. Combined optical model for micro-structured organic light emitting diodes. *Inf. MIDEM* **46**, 167–275 (2017).

[24] Kovačič, M., Jošt, M., Bokalič, M. & Lipovšek, B. Sklopljeno optično modeliranje sodobnih optoelektronskih gradnikov. *Elektrotehniski Vestn.* **87**, 223–234 (2020). http://www.dlib.si/stream/URN:NBN:SI:doc-2H1046ZZ/1ab9d4a8-6aab-40c3-abb5-9d826ff65672/PDF (in Slovene)

[25] Kovačič, M. *et al*. Analysis and optimization of light outcoupling in OLEDs with external hierarchical textures. *Opt. Express* **29**, 23701–23716 (2021). https://doi.org/10.1364/OE.428021

[26] Lipovšek, B., Krč, J. & Topič, M. Microtextured light-management foils and their optimization for planar organic and perovskite solar cells. *IEEE J. Photovolt.* **8**, 783–792 (2018). https://doi.org/10.1109/JPHOTOV.2018.2810844

[27] Jošt, M. *et al*. Efficient light management by textured nanoimprinted layers for perovskite solar cells. *ACS Photonics* **4**, 1232–1239 (2017). https://doi.org/10.1021/acsphotonics.7b00138

[28] Schmidt, T. D. *et al*. Emitter orientation as a key parameter in Organic Light-Emitting Diodes. *Phys. Rev. Appl.* **8**, 037001 (2017). https://doi.org/10.1103/PhysRevApplied.8.037001

[29] Hofmann, A., Schmid, M. & Brütting, W. The many facets of molecular orientation in organic optoelectronics. *Adv. Opt. Mater.* **9**, 2101004 (2021). https://doi.org/10.1002/adom.202101004

[30] Kim, K.-H. & Kim, J.-J. Origin and control of orientation of phosphorescent and TADF dyes for high-efficiency OLEDs. *Adv. Mater.* **30**, 1705600 (2018). https://doi.org/10.1002/adma.201705600

[31] Yokoyama, D. Molecular orientation in small-molecule organic light-emitting diodes. *J. Mater. Chem.* **21**, 19187–19202 (2011). https://doi.org/10.1039/C1JM13417E

[32] Schwab, T. *et al*. Highly efficient color stable inverted white top-emitting OLEDs with ultra-thin wetting layer top electrodes. *Adv. Opt. Mater.* **1**, 707–713 (2013). https://doi.org/10.1002/adom.201300241

[33] Schwab, T., Schubert, S., Müller-Meskamp, L., Leo, K. & Gather, M. C. Eliminating micro-cavity effects in white top-emitting OLEDs

by ultra-thin metallic top electrodes. *Adv. Opt. Mater.* **1**, 921–925 (2013). https://doi.org/10.1002/adom.201300392

[34] Zhang, W. *et al*. Rough glass by 3d texture transfer for silicon thin film solar cells. *Phys. Status Solidi C* **7**, 1120–1123 (2010). https://doi.org/10.1002/pssc.200982773

[35] Escarré, J., Söderström, K., Battaglia, C., Haug, F.-J. & Ballif, C. High fidelity transfer of nanometric random textures by UV embossing for thin film solar cells applications. *Sol. Energy Mater. Sol. Cells* **95**, 881–886 (2011). https://doi.org/10.1016/j.solmat.2010.11.010

[36] Meier, M. *et al*. UV nanoimprint for the replication of etched ZnO:Al textures applied in thin-film silicon solar cells. *Prog. Photovolt. Res. Appl.* **22**, 1226–1236 (2014). https://doi.org/10.1002/pip.2382

[37] Xiao, L., Su, S.-J., Agata, Y., Lan, H. & Kido, J. Nearly 100% internal quantum efficiency in an organic blue-light electro-phosphorescent device using a weak electron transporting material with a wide energy gap. *Adv. Mater.* **21**, 1271–1274 (2009). https://doi.org/10.1002/adma.200802034

[38] Dias, F. B. *et al*. Triplet harvesting with 100% efficiency by way of thermally activated delayed fluorescence in charge transfer OLED emitters. *Adv. Mater.* **25**, 3707–3714 (2013). https://doi.org/10.1002/adma.201300753

[39] Zhang, Q. *et al*. Nearly 100% internal quantum efficiency in undoped electroluminescent devices employing pure organic emitters. *Adv. Mater.* **27**, 2096–2100 (2015). https://doi.org/10.1002/adma.201405474

[40] Neyts, K. A. Simulation of light emission from thin-film microcavities. *J. Opt. Soc. Am. A* **15**, 962–971 (1998). https://doi.org/10.1364/JOSAA.15.000962

[41] Kovačič, M. Effect of dipole position and orientation on light extraction for red OLEDs on periodically corrugated substrate – FEM simulations study. *Inf. MIDEM* **51**, 73–84 (2021). https://doi.org/10.33180/InfMIDEM2021.105

[42] Lüder, H. & Gerken, M. FDTD modelling of nanostructured OLEDs: analysis of simulation parameters for accurate radiation patterns. *Opt. Quantum Electron.* **51**, 139 (2019). https://doi.org/10.1007/s11082-019-1838-4

[43] Lipovšek, B., Krč, J. & Topič, M. Optical model for thin-film photovoltaic devices with large surface textures at the front side. *Inf. MIDEM* **41**, 264–271 (2011). http://www.midem-drustvo.si/Journal%20papers/MIDEM_41%282011%294p264.pdf

[44] MATLAB – MathWorks (2022). https://www.mathworks.com/products/matlab.html

# Supplementary information (SI)

Table S1.
Optimal *EQE* and corresponding optimized layer thicknesses for devices without texturization – flat interfaces only.

| Anisotropy | 0 | 0.1 | 0.2 | 0.24 | 0.3 | 0.33 | 0.4 | 0.5 | 0.6 | 0.7 | 0.8 | 0.9 | 1 |
|---|---|---|---|---|---|---|---|---|---|---|---|---|---|
| *EQE* | 0.48 | 0.42 | 0.37 | 0.35 | 0.32 | 0.31 | 0.28 | 0.23 | 0.19 | 0.15 | 0.12 | 0.12 | 0.13 |
| **Glass (mm)** | 1.1 | 1.1 | 1.1 | 1.1 | 1.1 | 1.1 | 1.1 | 1.1 | 1.1 | 1.1 | 1.1 | 1.1 | 1.1 |
| **Layer (nm):** | | | | | | | | | | | | | |
| NPB | 34 | 32 | 31 | 33 | 29 | 31 | 30 | 30 | 28 | 100 | 86 | 84 | 86 |
| MoO₃ | 46 | 53 | 55 | 54 | 58 | 57 | 59 | 60 | 62 | 2 | 2 | 2 | 2 |
| Au | 2 | 2 | 2 | 2 | 2 | 2 | 2 | 2 | 2 | 2 | 2 | 2 | 2 |
| Ag | 17 | 16 | 16 | 16 | 16 | 16 | 16 | 16 | 16 | 8 | 13 | 16 | 16 |
| HTL | 46 | 44 | 42 | 42 | 42 | 42 | 42 | 42 | 41 | 58 | 84 | 135 | 138 |
| EBL | 10 | 10 | 10 | 10 | 10 | 10 | 10 | 10 | 10 | 10 | 10 | 10 | 10 |
| EML | 20 | 20 | 20 | 20 | 20 | 20 | 20 | 20 | 20 | 20 | 20 | 20 | 20 |
| HBL | 10 | 10 | 10 | 10 | 10 | 10 | 10 | 10 | 10 | 10 | 10 | 10 | 10 |
| ETL | 50 | 55 | 59 | 60 | 61 | 61 | 62 | 63 | 65 | 246 | 218 | 168 | 165 |
| Ag | 100 | 100 | 100 | 100 | 100 | 100 | 100 | 100 | 100 | 100 | 100 | 100 | 100 |

Table S2
Optimal *EQE* and corresponding optimized layer thicknesses for optimal coupling of light into the glass substrate,
considering an ideal extraction from the glass substrate into air. In simulations, the glass substrate is considered as half-infinitive –
expanded Table 1 from the main paper.

| Anisotropy | 0 | 0.1 | 0.2 | 0.24 | 0.3 | 0.33 | 0.4 | 0.5 | 0.6 | 0.7 | 0.8 | 0.9 | 1 |
|---|---|---|---|---|---|---|---|---|---|---|---|---|---|
| *EQE* | 0.8 | 0.73 | 0.68 | 0.65 | 0.62 | 0.6 | 0.56 | 0.51 | 0.47 | 0.45 | 0.47 | 0.48 | 0.5 |
| **Glass (mm)** | 1.1 | 1.1 | 1.1 | 1.1 | 1.1 | 1.1 | 1.1 | 1.1 | 1.1 | 1.1 | 1.1 | 1.1 | 1.1 |
| **Layer (nm):** | | | | | | | | | | | | | |
| NPB | 47 | 50 | 33 | 29 | 22 | 18 | 12 | 10 | 10 | 88 | 141 | 146 | 152 |
| MoO3 | 2 | 2 | 2 | 2 | 2 | 2 | 2 | 2 | 2 | 2 | 2 | 2 | 2 |
| Au | 2 | 2 | 2 | 2 | 2 | 2 | 2 | 2 | 2 | 2 | 2 | 2 | 2 |
| Ag | 4 | 5 | 4 | 4 | 4 | 4 | 4 | 4 | 4 | 4 | 4 | 4 | 5 |
| HTL | 39 | 41 | 37 | 37 | 37 | 37 | 37 | 36 | 33 | 202 | 168 | 168 | 170 |
| EBL | 10 | 10 | 10 | 10 | 10 | 10 | 10 | 10 | 10 | 10 | 10 | 10 | 10 |
| EML | 20 | 20 | 20 | 20 | 20 | 20 | 20 | 20 | 20 | 20 | 20 | 20 | 20 |
| HBL | 10 | 10 | 10 | 10 | 10 | 10 | 10 | 10 | 10 | 10 | 10 | 10 | 10 |
| ETL | 78 | 85 | 97 | 101 | 107 | 111 | 120 | 132 | 147 | 230 | 221 | 216 | 213 |
| Ag | 100 | 100 | 100 | 100 | 100 | 100 | 100 | 100 | 100 | 100 | 100 | 100 | 100 |

Table S3
Losses by layers with and without a three-sided pyramid texture.

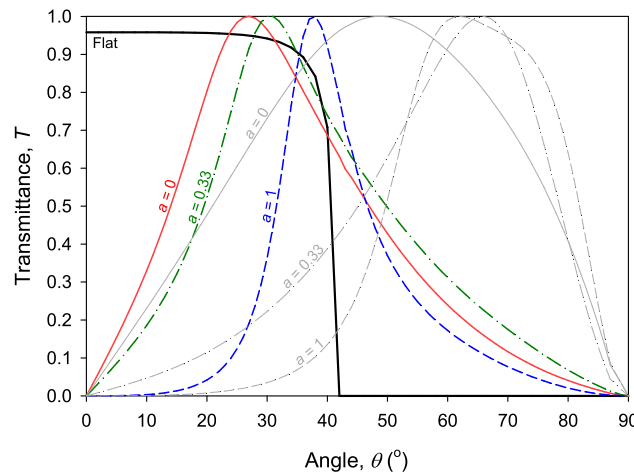| *a* = 0.24 | No texture | | With a three-sided pyramid texture | |
|---|---|---|---|---|
| | Optimal for flat | Optimal in glass | Optimal flat | Optimal in glass |
| *EQE* (%) | 35.0 | 17.1 | 37.2 | 51.0 |
| **(in glass)** | (53.7) | (65.1) | (53.7) | (65.1) |
| **Losses in layers (%):** | | | | |
| **Glass** | 10.5 | 33.9 | 0.1 | 0.1 |
| **Front contacts** | 25.9 | 15.3 | 30.5 | 14.5 |
| **Organic layers** | 10.4 | 14.1 | 11.8 | 13.8 |
| **Back contacts** | 18.2 | 19.6 | 20.4 | 20.6 |



**Fig. S1.**   Initial internal LID – optimized for a device with flat interfaces – coloured lines. Gray lines representing  the initial internal LID as optimized for optimal coupling of light into the glass substrate are added to show large differences between the two optimizations. Black line represents the angular-dependent transmission at the flat glass/air interface.
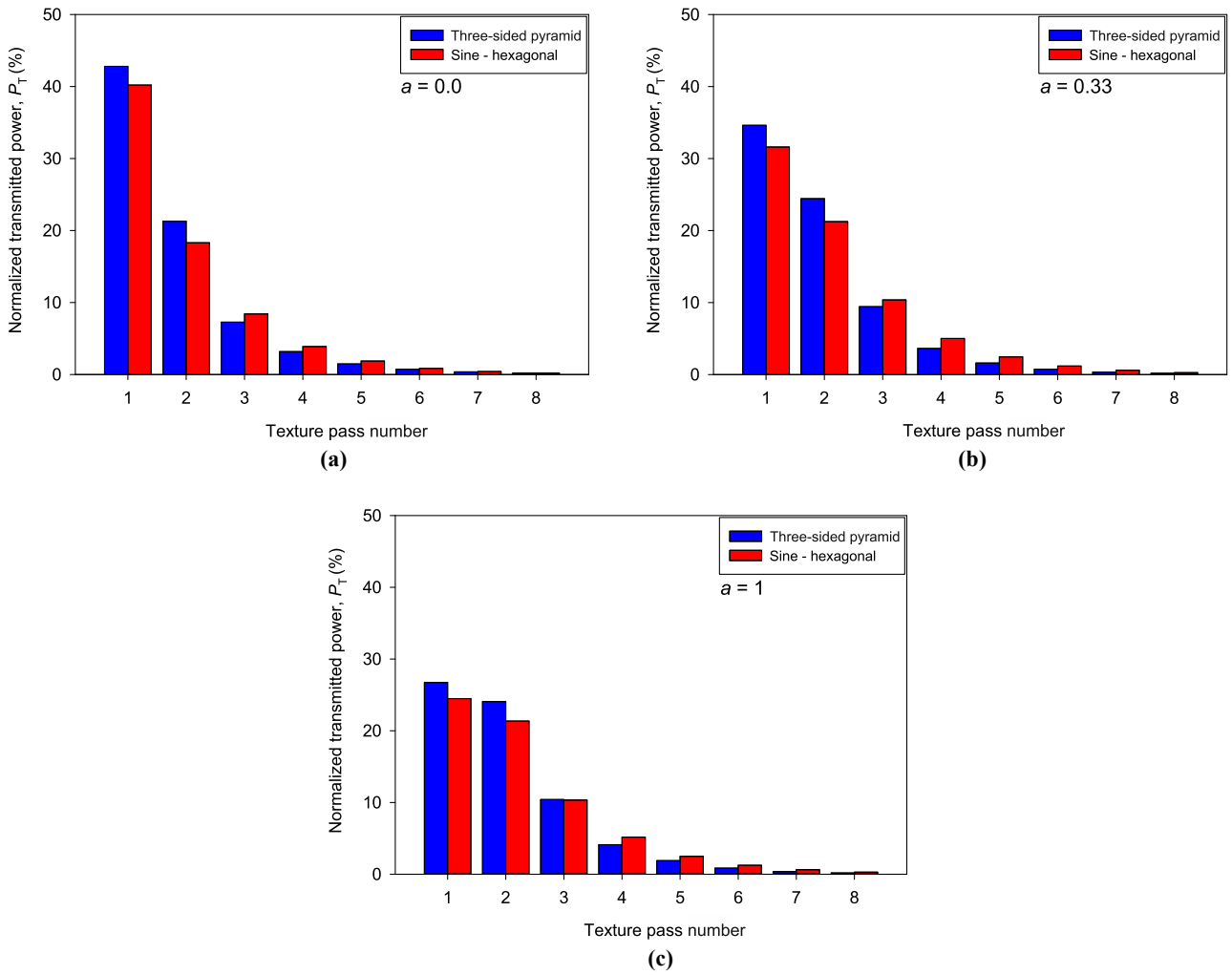
**(a)**



**(b)**



**(c)**

**Fig. S2.**   Transmitted power at each texture pass (optimized three-sided pyramids ($AR = 0.9$) for three different dipole orientations: ideally horizontal (a), isotropic (b), and ideally vertical (c). Values are normalized to the total power reaching the glass substrate (100%).
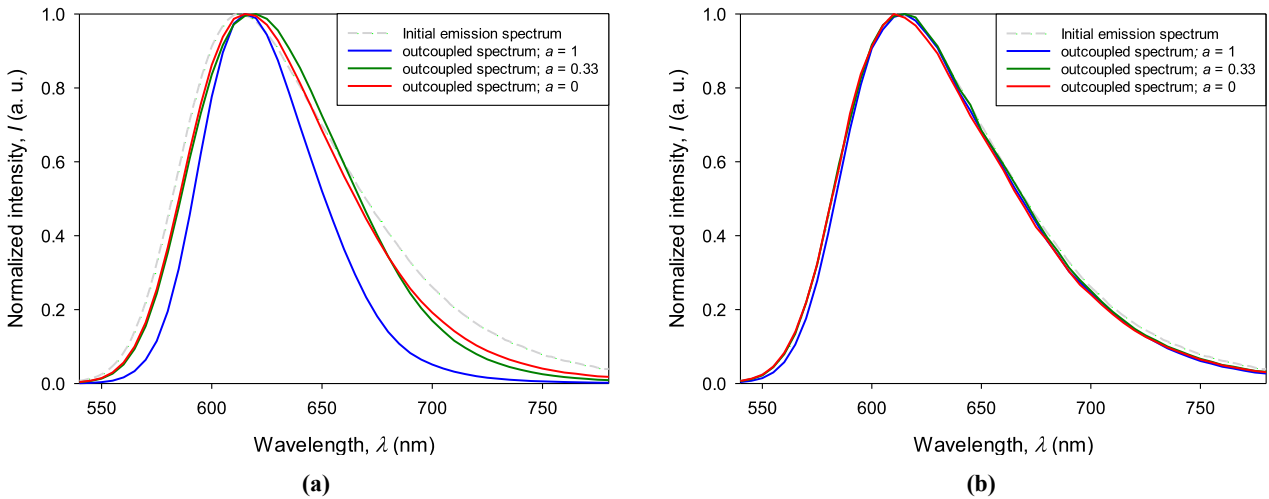


**(a)**



**(b)**

**Fig. S3.**   Normalized extracted intensity (in air) for OLEDs with different preferential orientation of dipoles for: flat interfaces (a) and optimized three-sided textures (b). The emission spectrum is indicated with by the grey dashed line.
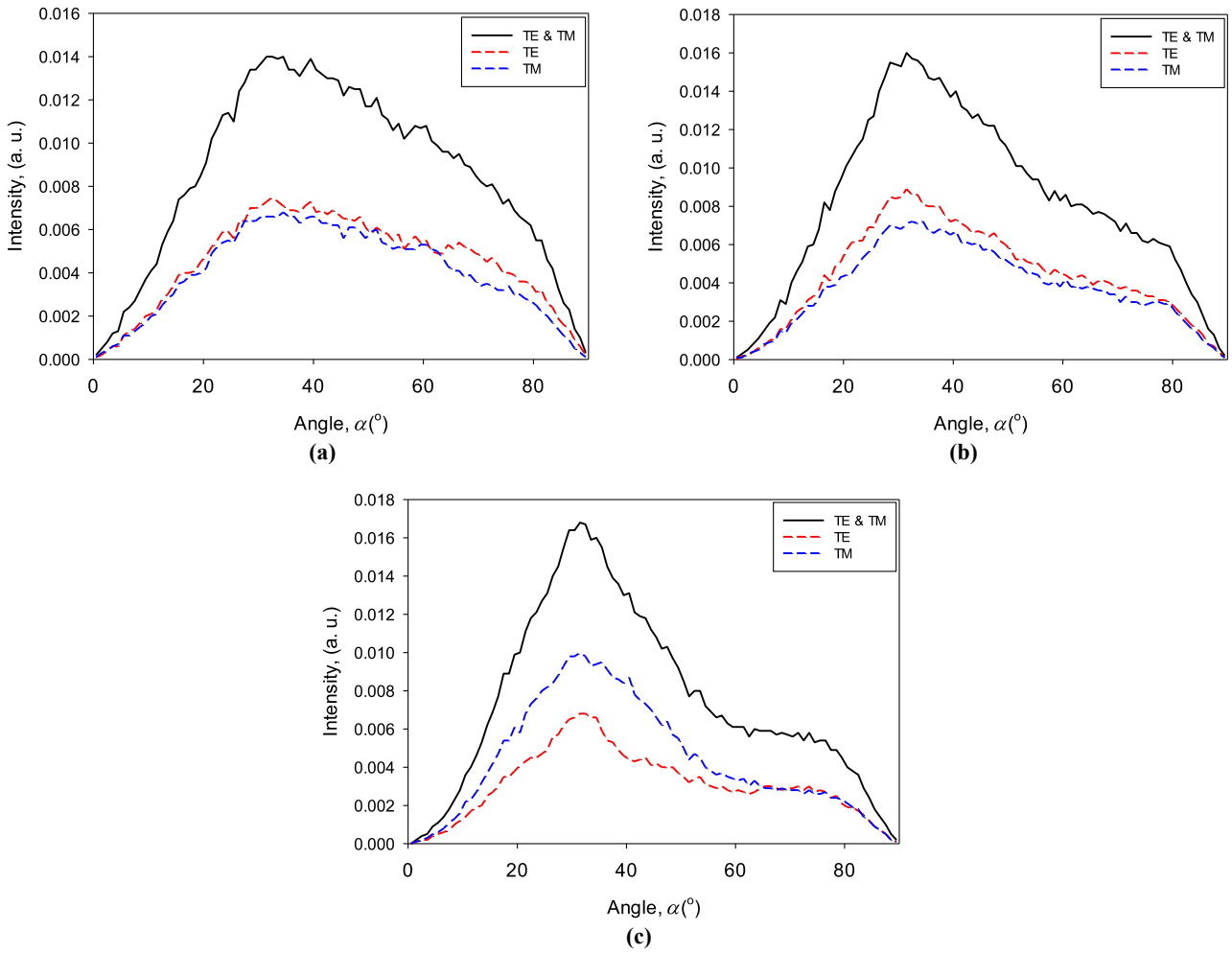
**Fig. S4**.    Integrated angular intensity distribution over azimuthal angles in air for devices with optimized three-sided pyramids, separated for TE, TM, and TE + TM polarization for: ideally horizontal (a), isotropic (b), and ideally vertical emission dipoles (c).
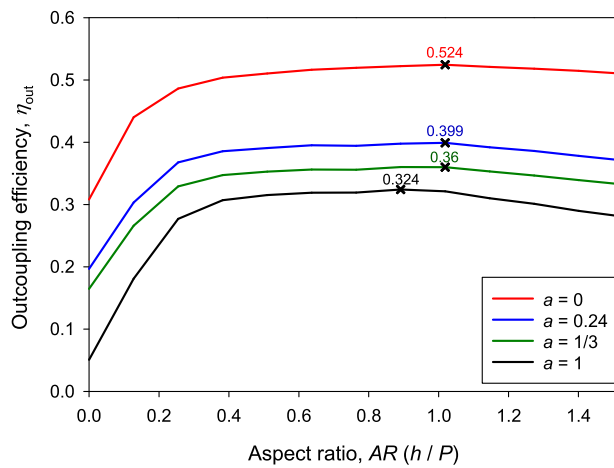


**Fig. S5.**    Outcoupling efficiency (*EQE*) by using the three-sided pyramid texture depending on the *AR* texture for 4 different preferential dipole orientations. An OLED device with an ITO contact is used here.